F-box protein MEC-15 promotes microtubule stability and neurite growth by antagonizing the HSP90 chaperone network in *Caenorhabditis elegans*

Chaogu Zheng[1,2,*,#], Emily Atlas[2], Ho Ming Terence Lee[1], Susan Laura Javier Jao[2], Ken C. Q. Nguyen[3], David H. Hall[3], and Martin Chalfie[2,*]

[1]School of Biological Sciences, The University of Hong Kong, Hong Kong SAR, China

[2]Department of Biological Sciences, Columbia University, New York, NY 10027, USA

[3]Department of Neuroscience, Albert Einstein College of Medicine, Bronx, NY 10461, U.S.A.

[*]Correspondence: cgzheng@hku.hk (C.Z.), mc21@columbia.edu (M.C.)

[#]Lead contact

Summary

Molecular chaperones often work collaboratively with the ubiquitination-proteasome system (UPS) to facilitate the degradation of misfolded proteins, which typically safeguards cellular differentiation and protects cells from stress. In this study, however, we report that the Hsp70/Hsp90 chaperone machinery antagonizes the activity of F-box protein MEC-15 to negatively regulate neuronal differentiation. Using the touch receptor neurons (TRNs) of *C. elegans*, we find that *mec-15(-)* mutants display defects in MT formation, neurite growth, synaptic development, and neuronal functions, and these defects can be rescued by the loss of Hsp70/Hsp90 chaperones and cochaperones. MEC-15 likely functions in a SCF complex to degrade DLK-1, which is an Hsp90 client protein stabilized by the chaperones. The abundance of DLK-1 and likely other Hsp90 substrates are fine-tuned by the antagonism between MEC-15 and chaperones, which regulates TRN development and synaptic functions of GABAergic motor neurons. Therefore, a balance between UPS and chaperones tightly controls neuronal differentiation.

Introduction

Molecular chaperones, including the heat shock proteins (Hsps), play essential roles in protein maturation, refolding, and degradation. Although the function of Hsps in the response to stress has been extensively characterized, their roles in neuronal differentiation are much less understood. Ishimoto et al. (1998) found that Hsp90 promotes neurite extension for the chick telencephalic neurons and spinal neurons *in vitro*. More recently, pharmacological inhibition of Hsp90 by 17-demethoxygeldanamycin (17-AAG) disturbed neuronal polarization and axonal elongation of cultured hippocampal neurons (Benitez et al., 2014). Hsp90 inhibition decreased expression of two Hsp90 client proteins, Akt and GSK3, which have diverse functions in cell differentiation. Thus, Hsp90 may regulate axon specification and growth by affecting specific signaling pathways through its chaperone activity. Given that the Hsp70 and Hsp90 chaperones interact with numerous client proteins, including transcription factors, kinases, and signaling molecules (Wayne et al., 2011), the regulation of neuronal morphogenesis by the chaperones is likely to be context-dependent. Whether Hsp70 and Hsp90 chaperones and their co-chaperones can also negatively regulate neurite growth, however, is unclear.

The ubiquitination-proteasome system (UPS) often works in concert with the chaperone-mediated refolding machinery for protein quality control, which promotes degradation of numerous misfolded proteins in a chaperone-dependent manner (Buchberger et al., 2010). In developing neurons, this process safeguards the protein quality of important guidance molecules. For example, the *C. elegans* BC-box protein EBAX-1, the substrate-recognition subunit of the Elongin BC-containing Cullin-RING ubiquitin ligase (CRL), and HSP-90/Hsp90 collaboratively regulate the folding and degradation of misfolded SAX-3/Robo receptor during axonal pathfinding (Wang et al., 2013). By preferentially binding to misfolded SAX-3, EBAX-1 not only recruits Hsp90 to promote the refolding of nonnative SAX-3 but also mediates the degradation of irreparable SAX-3 through CRL activity.

Despite known examples of collaboration, UPS and molecular chaperones could theoretically have opposing effects as well, since UPS increases normal protein turnover and chaperones can enhance protein stability. The antagonism of the UPS and the molecular chaperone machinery during neuronal differentiation, however, has not, to our knowledge, been

91 previously reported.

92 In this study, we find that the F-box and WD40 repeat domain-containing protein
93 MEC-15 (an ortholog of human FBXW9) and ubiquitination promote microtubule (MT)
94 stability and neurite growth by inhibiting the activity of the Hsp70/Hsp90 chaperone network.
95 Mutations in *mec-15* led to a range of developmental defects in the *C. elegans* touch receptor
96 neurons (TRNs), including the loss of microtubules (MTs), inhibited neurite growth and
97 branching, defects in localizing synaptic proteins, and the loss of sensory function. All these
98 defects in *mec-15* mutants can be rescued by removing the Hsp70 and Hsp90 chaperones and
99 co-chaperones, which unexpectedly suggests that the chaperones can disrupt neurite growth
100 and neuronal development and this activity is normally suppressed by the F-box protein and
101 the ubiquitination pathway. Downstream of the chaperones, we identified the MAP3 kinase
102 DLK-1 as an Hsp90 client protein that has MT-destabilizing activity and can inhibit neurite
103 growth. Therefore, our studies provided an important example of how molecular chaperones
104 are antagonized by the ubiquitination pathway during neuronal differentiation.

105

106 **Results**

107 **The F-box protein MEC-15 is required for MT stability and neurite growth**

108 The six *C. elegans* touch receptor neurons (ALML/R, PLML/R, AVM, and PVM) are
109 mechanosensory neurons that respond to gentle touch and have a simple morphology (Figure
110 1A-B). We previously identified a set of neomorphic tubulin mutations that caused the
111 formation of hyperstable MTs and the growth of an ectopic, posteriorly directed neurite in ALM
112 neurons (termed ALM-PN; similarly, ALM-AN is the anteriorly directed neurite of ALM;
113 PLM-AN and PLM-PN are the anteriorly and posteriorly directed neurites of PLM,
114 respectively; Zheng et al., 2017). Among those mutants, the β-tubulin *mec-7(u278;* C303Y*)*
115 allele had the strongest phenotype, with a very long ALM-PN extending to the tail region. By
116 suppressing this *mec-7(neo)* phenotype, we sought to identify genes that regulate MT stability
117 and neurite development. This *mec-7(u278)* suppressor screen (to be described elsewhere)
118 yielded a *mec-15* nonsense allele *u1042(*R26**)*, which completely suppressed the growth of
119 ALM-PN in *mec-7(u278)* mutants (Figure 1A-B). Another *mec-15* loss-of-function *(lf)* allele
120 *u75(*Q118**)* showed similar suppression. *mec-15* codes for a protein that contains a N-terminal

121 F-box and four WD-40 repeats (Figure 1C; Bounoutas et al., 2009b) and is orthologous to
122 human FBXW9.

123 The loss of *mec-15* also suppressed the growth of ectopic ALM-PN induced by other
124 mutations that increased MT stability and caused the formation of an ALM-PN (Figure 1C),
125 including another neomorphic β-tubulin mutation *mec-7(u1017;* L377F*)*, a *lf* mutation in a
126 destabilizing α-tubulin gene *tba-7*, and a *lf* mutation in a MT-depolymerizing kinesin-13 gene
127 *klp-7* (Zheng et al., 2017). These data suggest that MEC-15, a F-box protein, is generally
128 required for the excessive neurite growth triggered by elevated MT stability in TRNs.

129 MEC-15 is also required for normal TRN morphology. *mec-15(lf)* alleles *u75* and
130 *u1042* caused the shortening of both PLM-AN and PLM-PN in an otherwise wild-type
131 background (Figure 1D and S1). Another *mec-15* nonsense allele *u1008(*Q194**)*, isolated from
132 a different screen (Zheng et al., 2017), showed similar TRN morphological defects (Figure
133 S1A-C). Previous studies found that *mec-15* is required for touch sensitivity and the
134 localization of presynaptic proteins in TRNs (Bounoutas et al., 2009b). We found that the
135 ALM-AN and PLM-AN in *mec-15* mutants could not fully extend their synaptic branches
136 (Figure 1D, iv and v), which may have caused the synaptic defects.

137 As previously found (Bounoutas et al., 2009b; Sun et al., 2013), a *mec-15::GFP*
138 translational reporter was expressed in the TRNs, several head and tail neurons, and ventral
139 cord motor neurons (Figure 1E). We also generated a *mec-15::GFP* knock-in allele at the
140 endogenous *mec-15* locus through CRISPR/Cas9-mediated gene editing, but the resulted strain
141 did not have any detectable GFP expression, suggesting that the endogenous MEC-15 level
142 may be quite low. We next tested whether MEC-15 functions cell-autonomously in the TRNs.
143 Expression of wild-type *mec-15(+)* from the TRN-specific *mec-18* promoter rescued both the
144 neurite growth defects in *mec-15(lf)* single mutants and the loss of ALM-PN in *mec-15*(*lf);*
145 *mec-7(u278 neo)* double mutants. In contrast, the expression of MEC-15 with some or all of
146 the F-box domain removed could not rescue either phenotype (Figure 1C and S1), suggesting
147 that MEC-15 functions within the TRNs and its activity requires the F-box domain.

148 F-box proteins assemble with Skp and Cullin proteins to form SCF E3 ubiquitin ligase
149 complexes. The involvement of ubiquitination in the action of MEC-15 was supported by the
150 findings that TRN-specific knockdown of *uba-1*, the only known *C. elegans* gene encoding a

151 ubiquitin-activating enzyme, strongly suppressed the growth of ALM-PN in *mec-7(u278 neo)*
152 mutants (Figure S1D). Because mutation or general knockdown of *uba-1* causes sterility and
153 lethality, we performed cell-specific RNAi by expressing double-stranded RNA (dsRNA)
154 against *uba-1* from the TRN-specific *mec-17* promoter. As a negative control, expression of
155 dsRNA against GFP did not affect neurite growth. Moreover, inhibition of proteasomes by
156 bortezomib partially suppressed the growth of ALM-PN (Figure S1D). In addition, previous
157 work found that MT depolymerization led to a general reduction in protein levels in TRNs
158 (Bounoutas et al., 2011). We found that mutations in *mec-15*, knockdown of *uba-1*, and
159 bortezomib treatment all significantly reduced TagRFP expression from a *mec-17p::TagRFP*
160 transgene in the TRNs, measured as fluorescent intensity (Figure S1E). The above data lead to
161 the hypothesis that some MT-destabilizing molecule, which is normally ubiquitinated and
162 targeted for degradation by MEC-15, became abnormally accumulated in the *mec-15*-deficient
163 TRNs, leading to reduced MT stability and the inhibition of neurite growth.

164 Although reduced *uba-1* activity affected ALM-PN outgrowth, we could not identify
165 the other components of the putative SCF complex. In fact, our results suggest that these other
166 components may be redundant. For example, although we found that MEC-15 physically
167 interacted with the Skp homolog SKR-1 in a yeast two-hybrid assay (Figure S1F), *skr-1(ok1696)*
168 null mutations did not cause TRN morphological defects and did not suppress ALM-PN in
169 *mec-7(u278 neo)* mutants. In addition, RNAi of *skr-2, skr-8, skr-9, skr-12,* and *skr-13* (other
170 Skp homologs) did not suppress *mec-7(neo)* phenotype (see Materials and Methods for details).
171 Cullin, the third component of the SCF complex, also appeared to be redundant, since
172 mutations or knockdown of Cullin homologs *cul-1*, *cul-2*, *cul-4*, *cul-5*, and *cul-6* did not induce
173 the same defect as the loss of MEC-15.

174 **Loss of molecular chaperones suppresses neurite growth defects of *mec-15* mutants**

175 To identify the downstream target(s) of the MEC-15-dependent ubiquitination
176 pathway, we screened for suppressors of *mec-15* in the *mec-15(u1042); mec-7(u278)*
177 background and identified the phenotype-causing mutations in eight mutants with restored
178 ectopic ALM-PNs (STAR methods and Table S1). Among those mutants were one recessive *lf*
179 allele of *sti-1* and four recessive *lf* alleles of *pph-5*. *sti-1* encodes a homolog of the Sti1/Hop
180 cochaperone that physically links Hsp70 and Hsp90 through the tetratricopeptide repeat (TPR)-

181 domain (Schmid et al., 2012), and *pph-5* encodes a homolog of Protein Phosphatase 5 (PP5), a
182 TPR-domain containing serine/threonine phosphatase that binds to Hsp90 and activates its
183 kinase clients (Vaughan et al., 2008). Deletion alleles of both genes [*sti-1(ok3354)* and *pph-*
184 *5(ok3498)*] also induced the growth of ALM-PN in *mec-15(u1042); mec-7(u278)* animals
185 (Figure 2A-C and Table S1).

186 Since STI-1 and PPH-5 are components of the molecular chaperone pathway, we
187 tested other genes in the same pathway. The removal of *hsp-90* (a Hsp90 homolog) and *hsp-*
188 *110* (a Hsp70 family member) but not *hsp-1* (another Hsp70 family protein) suppressed the loss
189 of MEC-15. *hsp-90(ok1333)* and *hsp-110(gk533)* deletion alleles caused larval arrest, but the
190 arrested *mec-15(u1042); hsp-90(ok1333); mec-7(u278)* and *mec-15(u1042); hsp-110(gk533);*
191 *mec-7(u278)* triple mutants had long ALM-PNs (Figure 2C).

192 Moreover, TRN-specific knockdown of *hsf-1/*heat shock transcription factor 1, which
193 activates the expression of Hsps and functions upstream of HSP-90 and HSP-110 (Singh and
194 Aballay, 2006), also induced the growth of ALM-PNs in *mec-15(u1042); mec-7(u278)* double
195 mutants (Figure 2C). PP5, the PPH-5 homolog, dephosphorylates the co-chaperone Cdc37 in
196 yeast and mammals, which is essential for the folding and maturation of Hsp90-dependent
197 protein kinases (Vaughan et al., 2008; Wandinger et al., 2006). TRN-specific RNAi silencing
198 of *cdc-37*, *C. elegans* Cdc37, promoted the growth of ALM-PN in *mec-15(-); mec-7(u278)*
199 animals (Figure 2C), suggesting that some Hsp90 kinase clients may be involved in the
200 regulation of neurite growth.

201 Through a candidate RNAi screen of 27 Hsp70/Hsp90-related genes (Table S2), we
202 found that knocking down *daf-41*, which encodes the Hsp90 co-chaperone PTGES3/p23, also
203 restored the growth of ALM-PNs in *mec-15(u1042); mec-7(u278)* animals (Figure S2C). *daf-*
204 *41(ok3052)* deletion allele showed the same phenotype (Figure 2C). Thus, disrupting the
205 Hsp70/Hsp90 chaperone machinery by deleting either Hsp70, Hsp90, p23, Sti1/Hop, PP5, or
206 Cdc37 rescued the loss of the F-box protein MEC-15.

207 Importantly, the suppression of *mec-15* loss did not depend on the presence of *mec-*
208 *7(u278 neo)*. We crossed *lf* alleles of *hsp-110*, *hsp-90*, *daf-41/p23*, *sti-1*, and *pph-5* with *mec-*
209 *15(u1042)* to create double mutants and found that the shortening of PLM-PN in *mec-15* single
210 mutants was suppressed in all double mutants (Figure 2E and G). TRN-specific knockdown of

211 *cdc-37* had similar effects (Figure 2G). In addition, we found that the PLM-AN outgrowth
212 defect (but not PLM-PN) in *mec-15* null mutants was more severe at 25°C than at 20°C (Figure
213 S2A), suggesting that the abnormally accumulated proteins may have higher expression or
214 exert a stronger MT-destabilizing activity at higher temperature. This more severe PLM-AN
215 growth defects at 25°C was also suppressed in *mec-15; daf-41*, *mec-15; sti-1*, and *mec-15; pph-*
216 *5* double mutants; most PLM-ANs extended fully and grew beyond the vulva (Figure 2F). We
217 could not measure the length of PLM-AN in *mec-15; hsp-110* and *mec-15; hsp-90* adults,
218 because those double mutants arrested at early larval stages.

219 HSP-90 and the cochaperones DAF-41, STI-1, and PPH-5 are expressed in most *C.*
220 *elegans* cells (Gillan et al., 2009; Richie et al., 2011; Song et al., 2009), and we confirmed their
221 expression in the TRNs (Figure S3A-C). Moreover, we were able to rescue the loss of *daf-41*,
222 *sti-1*, and *pph-5* in their double mutants with *mec-15(u1042)* and their triple mutants with *mec-*
223 *15(u1042); mec-7(u278)* by expressing the wild-type cochaperone gene from a TRN-specific
224 *mec-17* promoter, indicating that the chaperone pathway genes function cell-autonomously in
225 the TRNs (Figure S3D). Unexpectedly, mutants of chaperones and cochaperones also had
226 strong maternal effects in suppressing the Mec-15 phenotype (Figure S4; see Supplemental
227 Results for details).

228 Because mutations in *sti-1* and *pph-5* showed strong and almost identical suppression
229 of the *mec-15(-)* phenotype, we wondered whether the two genes interact with each other. Rohl
230 et al. (2015) previously found that the phosphorylation of yeast Sti1 and human Hop, STI-1
231 homologs, inhibited their cochaperone activity, we found that phosphorylation of *C. elegans*
232 STI-1 inhibited its activity in regulating neurite growth. TRN-specific expression of non-
233 phosphorylatable, hyperactive STI-1 mutants suppressed the growth of ALM-PN in *mec-*
234 *7(u278)* animals, and the expression of phosphomimic, inactive STI-1 mutants restored ALM-
235 PN growth in *mec-15(u1042); mec-7(u278)* animals. Non-phosphorylatable STI-1 mutants also
236 suppressed the rescuing effects of *pph-5* mutations in *mec-15; mec-7* animals, suggesting that
237 PPH-5 may enhance STI-1 activity through dephosphorylation (Figure S5; see Supplemental
238 Results for details).

239 Moreover, *hsp-110*, *hsp-90*, *daf-41*, *sti-1*, and *pph-5* single mutants did not show any
240 TRN morphological defects and did not cause touch insensitivity, suggesting that their

241 activities are normally not required for TRN differentiation and function. Nevertheless, an
242 inhibitory role for these Hsp70/Hsp90 chaperones and cochaperones on TRN differentiation is
243 revealed when *mec-15* is lost, because the chaperone proteins were required for the disruption
244 of TRN morphology and functions in *mec-15(-)* mutants.

245 **Mutations in chaperones rescues MT loss and synaptic defects of *mec-15* mutants**

246 Consistent with the hypothesis that chaperones are detrimental for TRN development
247 in *mec-15* mutants, we also observed suppressing effects of chaperone mutations on *mec-15(lf)*-
248 induced changes in MT organization. We previously showed that MT organization and stability
249 determined neurite growth patterns in TRNs (Zheng et al., 2017). Using electron microscopy
250 (EM), we found that the number of MTs in a cross section of TRN neurite is dramatically
251 reduced in *mec-15* mutants compared to the wild type in both ALM and PLM (Figure 3A-B).
252 For example, PLM-AN in *mec-15(u1042)* mutants had 4.9 ± 2.9 (mean ± SD) MTs on average
253 in a cross section, compared to 29.8 ± 6.5 MTs in the wild type. In addition to the loss of MTs,
254 *mec-15* mutants also had smaller MTs than the wild type. For example, whereas 98% (N = 306)
255 of the MTs in the wild type had the 15-protofilament (15-p) MTs, 71% (N = 65) of the MTs in
256 the PLM-AN of *mec-15(u1042)* adults had between 11 and 13 protofilaments, resulting in
257 significantly smaller MT diameters (Figure 3C-D). The loss of MTs and the smaller size
258 indicate that MTs are highly unstable and disorganized in the absence of MEC-15.

259 The structural defects of MTs in *mec-15* mutants are rescued in *mec-15; sti-1* and *mec-*
260 *15; pph-5* double mutants, which had restored MT numbers, 16.2 ± 4.3 and 17.6 ± 9.2 MTs in
261 the PLM-AN, respectively. The double mutants also have large-diameter 15-protofilament MTs,
262 similar to those seen in the wild type (Figure 3D). These data suggest that the loss of Hsp90
263 co-chaperones promotes MT formation and stability, which in turn rescues the TRN neurite
264 growth defects in *mec-15* mutants.

265 Since MT depolymerization in the TRNs causes a general reduction in protein levels
266 (Bounoutas et al., 2011), *mec-15* mutants showed drastically decreased TagRFP expression
267 from a *mec-17p::TagRFP* transgene in the TRNs, compared to the wild type; this reduction in
268 protein level was completely rescued by mutations in *daf-41/p23*, *sti-1*, and *pph-5* (Figure 3E).
269 Moreover, *mec-15* mutants also showed almost complete loss of GFP::RAB-3 localization at
270 the presynaptic site in PLM neurons and partial loss in ALM neurons (Bounoutas et al., 2009b).

271 This transport defect is likely caused by unstable MTs and is suppressed by the mutations in
272 *sti-1* and *pph-5* (Figure 3F).

273 TRNs are mechanosensory neurons that detect gentle body touches; this sensory
274 function of TRNs depends on the 15-p MTs (Bounoutas et al., 2009a). Mutations in *mec-15*
275 cause touch insensitivity (Chalfie and Au, 1989), likely due to the loss of 15-p MTs. This
276 sensory defect was fully rescued in *sti-1; mec-15* and *pph-5; mec-15* double mutants and
277 partially rescued in *daf-41; mec-15* double mutants (Figure 3G).

278 Thus, in addition to neurite development, the removal of the molecular chaperone
279 pathway genes restored a variety of MT-related structures and functions affected by *mec-15*
280 loss. Given the protective nature of the chaperones, this restoration is rather unexpected and
281 suggests that Hsp70/Hsp90 machinery may contribute to the refolding and stabilization of a
282 client protein or proteins that negatively affects MT stability and TRN development.

283 **Hsp90 chaperones inhibit neurite growth by stabilizing DLK-1**

284 Since our *mec-15* suppressor screen (Table S1) yielded two *dlk-1 lf* alleles, *u1105*
285 (V844I) and *u1138* (W394*), we examined the possibility that Hsp70/Hsp90 might regulate
286 MT organization and neurite growth by acting on *dlk-1*, which encodes a MAP3 kinase
287 homologous to human MAP3K12 and MAP3K13. Both *u1105* and *u1138* mutations restored
288 the growth of both ALM-PN and PLM-PN in *mec-15(u1042); mec-7(u278)* mutants (Figure
289 4A and B). The missense mutation (V844I) in *u1105* is adjacent to a C-terminal region (aa 850-
290 881) of DLK-1 that interacts with its kinase domain (Yan and Jin, 2012); so, catalytic function
291 of DLK-1 may be impaired in *u1105* mutants. Another *dlk-1 lf* allele, *ju476* (a frameshift
292 mutation), suppressed *mec-15(-)* even more strongly. The phenotype of *dlk-1(-)* is similar to
293 the effects of *sti-1(-)* and *pph-5(-)* in *mec-15; mec-7* mutants. Independent of the *mec-7(u278)*
294 background, *dlk-1 lf* alleles also suppressed the shortening of PLM-PN and the premature
295 termination of PLM-AN in *mec-15(u1042)* mutants (Figure 4C and D). Moreover, *dlk-1 lf*
296 alleles showed maternal effects similar to *daf-41*, *sti-1,* and *pph-5 lf* alleles (Figure 4B). These
297 data suggest that *dlk-1* may function in the same pathway as the chaperone and co-chaperone
298 genes.

299 Expression of DLK-1a from the TRN-specific *mec-17* promoter rescued the loss of
300 *dlk-1* by suppressing the growth of ALM-PN in *dlk-1; mec-15; mec-7* triple mutants,

301 confirming that DLK-1 functions cell-autonomously (Figure 4E). More importantly,
302 overexpression of DLK-1a also suppressed the phenotype of *pph-5* and *sti-1* mutants,
303 indicating that DLK-1 functions downstream of the chaperones (Figure 4E). Through a yeast
304 two-hybrid assay, we detected a physical interaction between HSP90 and DLK-1a (Figure 4F),
305 which is the long and active isoform of DLK-1 (Yan and Jin, 2012). Moreover, the level of
306 GFP::DLK-1a fusion protein is drastically reduced in *pph-5* and *sti-1* mutants, suggesting that
307 the stability of DLK-1 relies on the Hsp90 chaperones (Figure 4G).

308 DLK-1 is known to induce MT dynamics and is essential for axonal regeneration in
309 TRNs (Tang and Chisholm, 2016; Yan et al., 2009); DLK-1 signaling is also required for MT
310 depolymerization-induced downregulation of protein levels in TRNs (Bounoutas et al., 2011).
311 Indeed, *dlk-1 lf* mutations blocked the downregulation of TagRFP in *mec-15(-)* animals, while
312 overexpression of DLK-1a in the wild-type animals led to marked reduction of TagRFP
313 expression (Figure 4H). Consistent with a role in reducing MT stability, DLK-1a
314 overexpression strongly suppressed the growth of ectopic ALM-PN in *mec-7(u278)* animals
315 and also shortened PLM-AN and PLM-PN in wild-type animals (Figure 4C and E). The above
316 data suggest that DLK-1 likely mediates the activity of Hsp90 chaperones and cochaperones in
317 destabilizing MTs during development. Coincidentally, a recent study found that Hsp90 is also
318 a chaperone for DLK in mouse neurons and in Drosophila and is required for axon injury
319 signaling (Karney-Grobe et al., 2018). Thus, the regulation of DLK-1 by Hsp90 chaperone
320 appears to be evolutionarily conserved.

321 Importantly, DLK-1 is not the only downstream effector of the chaperones, because
322 unlike the *sti-1* and *pph-5 lf* mutations, the *dlk-1 lf* mutations did not rescue the touch
323 insensitivity, PLM-AN branching defects, or the GFP::RAB-3 localization defect in *mec-15*
324 mutants (Figure S6). Even for neurite growth, the loss of *dlk-1* did not fully rescue the
325 outgrowth defect of PLM-PN and PLM-AN in *mec-15* mutants (Figure 4C and D). Thus, we
326 expect that other Hsp90 client proteins also function during TRN development.

327 **MEC-15 downregulates DLK-1 levels in TRNs**

328 Since MEC-15 is a F-box protein that likely functions in a SCF complex to target
329 substrate protein for ubiquitination and degradation, we next asked whether MEC-15 regulates
330 DLK-1 protein levels. We found that the expression of GFP::DLK-1 fusion proteins was

elevated in *mec-15* mutants (Figure 4G), whereas the levels of STI-1::GFP and PPH-5::GFP fusion proteins were not changed in *mec-15* mutants (Figure S7A). Importantly, the level of GFP::DLK-1 was also increased by blocking ubiquitination through TRN-specific silencing of *uba-1* (Figure 4G). Thus, MEC-15 likely targets DLK-1 but not the Hsp90 co-chaperones for degradation.

We could not detect any physical interaction of MEC-15 with DLK-1a in yeast two-hybrid assays, suggesting that the interaction may be transient or dependent on particular post-translational modification of DLK-1. We did not detect any interaction of MEC-15 with STI-1, PPH-5, DAF-41, HSP-90, or HSP-110 either. In attempts to detect MEC-15 binding to DLK-1 in the TRNs, we made constructs that express HA-tagged MEC-15 and FLAG-tagged DLK-1 from the TRN-specific *mec-18* and *mec-17* promoters, respectively. When injected separately, both MEC-15 and DLK-1 can be detected by western blot probing the tags; but when injected together, only MEC-15::HA was detected, and FLAG::DLK-1 was undetectable (Figure S7B). Although this renders the co-immunoprecipitation assay impossible, these results suggested that MEC-15 suppressed the expression of DLK-1 at the protein level.

RPM-1, a RING-finger E3 ubiquitin ligase, also downregulates the abundance of DLK-1 at the protein level and modulates the p38 MAP Kinase pathway (Nakata et al., 2005). The phenotype of *rpm-1* mutants, however, is the direct opposite of *mec-15* mutants. Instead of the shortened TRN neurites of *mec-15* mutants, *rpm-1(ok364)* knockout mutants had overextended ALM-AN and PLM-AN (Figure S7C; Schaefer et al., 2000). Moreover, the loss of *rpm-1* did not suppress the ectopic ALM-PN in *mec-7(u278)* mutants, and the *rpm-1 mec-7* double mutants showed both long ALM-PN and the overextension of ALM-AN and PLM-AN (Figure S7D-F). Thus, RPM-1 appears to negatively regulate neurite growth, whereas MEC-15 promotes growth. Downstream of both proteins, DLK-1 may exert dual functions in both inducing MT dynamics and promoting neurite extension depending on the cellular contexts.

mec-15 is epistatic to *rpm-1*, since *mec-15; rpm-1* double mutants showed mostly the *mec-15(-)* phenotype, having shortened PLM-ANs and PLM-PNs. The *mec-15; rpm-1; mec-7* triple mutants showed the phenotype of *mec-15; mec-7* double mutants in the suppression of ALM-PN (Figure S7E-F). This epistasis suggests that either MEC-15-mediated regulation of DLK-1 plays a more dominant role in TRNs than RPM-1-mediated regulation or MEC-15-

regulated DLK-1-independent pathways act downstream of RPM-1-controlled pathways.

MEC-15 regulates the function of GABAergic motor neuron by antagonizing Hsp90 chaperone activities

Finally, the genetic interaction between *mec-15* and the Hsp90 chaperones occurs not only in the TRNs, but also in other neurons. In the ventral cord motor neurons, MEC-15 regulates the trafficking of synaptic vesicle protein SNB-1 and promotes GABAergic synaptic transmission (Sun et al., 2013). We found that compared to the wild-type animals, *mec-15* mutants had fewer synaptic puncta labeled by SNB-1::GFP in GABAergic neurons, and this deficit in synaptic density was rescued by mutations in *sti-1* or *pph-5*, although the average fluorescent intensity of each puncta was similar between the mutants and the wild-type animals (Figure 5A-C).

Behaviorally, reduced GABA release in *mec-15* mutants led to lower inhibitory postsynaptic currents in the body wall muscles and increased sensitivity to the acetylcholine esterase inhibitor aldicarb, which causes paralysis through the accumulation of acetylcholine and persistent muscle contraction (Sun et al., 2013). This increased sensitivity to aldicarb in *mec-15* mutants was completely suppressed in *mec-15; sti-1* and *mec-15; pph-5* mutants (Figure 5D). Therefore, MEC-15 and Hsp90 chaperones also appear to counter each other to regulate GABAergic synaptic function. Moreover, similar to the thermosensitive PLM-AN growth defects in *mec-15* mutants, we found that *mec-15(-)* animals grown at 25°C are much more sensitive to aldicarb than animals raised at 20°C; loss of *sti-1* or *pph-5* also rescued this temperature-dependent defects (Figure 5D). This result suggests that MEC-15 target proteins in both TRNs and GABAergic motor neurons are more stable or have higher levels at higher temperature, likely due to the increased activity of Hsp90 chaperones at higher temperature.

Discussion

Ubiquitination and protein degradation promote stable MTs and neurite growth

The ubiquitination-proteasome system (UPS) affects many processes of neuronal development, including neurogenesis, cell fate specification, neuronal migration, polarization, and axonal and dendrite morphogenesis (Tuoc and Stoykova, 2010; Yamada et al., 2013). With respect to neurite morphogenesis, previous studies suggested that E3 ubiquitin ligase can both

391 positively and negatively regulate neurite growth. For example, during axodendritic
392 polarization in hippocampal neurons, the HECT-domain E3 ubiquitin ligase Smurf1 promotes
393 the growth of axons by degrading RhoA (inhibitor of axon growth), whereas Smurf2 inhibits
394 the growth of neurites fated to be dendrites by degrading Ras GTPase Rap1B (inducer of
395 neurite growth; (Cheng et al., 2011; Schwamborn et al., 2007).

396 Our studies identified the F-box and WD40 domain protein MEC-15 (ortholog of
397 human FBXW9) as a positive regulator of neurite growth. As in the above examples, MEC-15
398 presumably functions in a Skp, Cullin, F-box containing complex (or SCF complex), which is
399 a E3 ubiquitin ligase, to degrade some protein(s) that can inhibit neurite outgrowth. One
400 potential substrate of MEC-15 is the MAP3 kinase DLK-1, which is known to induce MT
401 dynamics (Tang and Chisholm, 2016) and can suppress neurite growth when overexpressed
402 (this study). Since the loss of *dlk-1* did not fully rescue the developmental defects of *mec-15(-)*
403 mutants, MEC-15 likely has multiple substrates.

404 In the PLM neurons, the anterior neurite is considered an axon because its MTs has
405 uniform "plus-end out" polarity, whereas the posterior neurite is more like a dendrite given that
406 its MTs have mixed polarity (Hsu et al., 2014). MEC-15 is required for the extension of both
407 PLM-AN and PLM-PN, which suggests that MEC-15 is a general regulator of neurite growth
408 instead of an axon- or dendrite-specific regulator, like the E3 ligase Cdh1-APC and Cdc20-
409 APC (Konishi et al., 2004). This function of MEC-15 may be attributed to its activity in
410 promoting the formation of stable MTs, since mutations in *mec-15* led to significant loss of
411 MTs and the reduction of MT diameters. Thus, our studies link SCF complex and UPS to the
412 general stability of MT cytoskeletons.

413 **Dual yet contradictory functions of DLK-1**

414 Another conserved RING-domain E3 ubiquitin ligase, RPM-1, also regulates neurite
415 extension in TRNs by interacting with the SCF complex, including SKR-1/Skp, CUL-1/Cullin,
416 and the F-box protein FSN-1/FBXO45 (Nakata et al., 2005). However, MEC-15 and RPM-1
417 have opposing functions. MEC-15 promotes neurite growth, whereas RPM-1 inhibits neurite
418 growth. More surprisingly, both RPM-1 and MEC-15 appear to target DLK-1 for degradation.
419 Since mutations in *dlk-1* partially suppress both the overextension phenotype in *rpm-1(-)*
420 mutants (Nakata et al., 2005) and the underextension in *mec-15(-)* mutants (this study), DLK-

421 1 may exhibit dual yet opposite functions in regulating neurite growth.

422 Elevated DLK-1 level promotes axon growth in *rpm-1(-)* mutants but inhibits neurite
423 growth in *mec-15(-)* mutants; these two opposing functions seem to be balanced under normal
424 conditions, since *dlk-1(-)* mutants did not show any TRN morphological defects. Perhaps the
425 spatial and temporal expression of DLK-1 determines which of the two opposing functions is
426 engaged. For example, DLK-1 may play inhibitory roles for general neurite extension during
427 the growth phase by reducing MT stability globally in the entire cell and then prevent axon
428 termination at specific sites at a later stage of development. Because *mec-15(-) rpm-1(-)* double
429 mutants exhibited the underextension phenotype, the overall effects of accumulating DLK-1
430 appear to inhibit neurite growth. Interestingly, DLK-1 also initiates apparently contradictory
431 responses under stress conditions during development and after axonal injury (Tedeschi and
432 Bradke, 2013). For example, after optical nerve injury in mice, DLK triggers the expression of
433 both proapoptotic and regenerative genes, although cell death is the dominant response
434 (Watkins et al., 2013). Future studies are needed to understand how the multifaceted functions
435 of DLK-1 are controlled spatially and temporally to initiate specific signalling. Our work
436 suggests that different components of the UPS could generate distinct cellular responses by
437 targeting the same protein.

438 **Inhibitory role of Hsp70/Hsp90 chaperones and co-chaperones in neuronal development**

439 Besides the protective effects of Hsps in cells under stressed conditions, growing
440 evidence suggest that these chaperones also play regulatory roles in normal neurodevelopment
441 (Miller and Fort, 2018). The ATP-dependent Hsp70 and Hsp90 family chaperones are
442 expressed in the nervous system during mouse embryonic and postnatal development, which
443 suggests that they may function in both neurogenesis and late-stage neurodevelopment (Loones
444 et al., 2000). In fact, deletion of the transcription factor HSF1, which activates the transcription
445 of many Hsps genes, in mice led to impaired olfactory neurogenesis and hippocampal
446 spinogenesis and neurogenesis (Uchida et al., 2011), supporting a critical role for Hsps in
447 proper neurodevelopment.

448 At the subcellular level, Hsc70 (Hsp70 family chaperone) and Hsp90 are localized to
449 the apical dendrites of Purkinje cells and cerebellar neurons from postnatal period into
450 adulthood (D'Souza and Brown, 1998); in the differentiating hippocampal neurons, Hsp90 was

451 associated with the cytoskeleton in branch points and terminal ends (Quinta and Galigniana,
452 2012). These results suggest that Hsps may regulate neuronal polarization and neurite
453 morphogenesis by modulating cytoskeleton dynamics. Indeed, pharmacological inhibition of
454 Hsp90 disturbed the polarization and axonal extension of cultured hippocampal neurons by
455 inhibiting the PI3K/Akt/GSK3 signaling pathway (Benitez et al., 2014), which is known to
456 regulate neuronal morphogenesis (Kim et al., 2011). The fact that Akt and GSK3 are Hsp90
457 client proteins (Banz et al., 2009; Sato et al., 2000) indicates that Hsp90 could regulate cell
458 differentiation by maintaining the stability of its client proteins. Thus, given that Hsp90
459 interacts with hundreds of client proteins, the specific function of Hsp90 in differentiation
460 would depend on the function of its client protein(s) in particular cellular contexts.

461 Our studies identified one such context, in which Hsp70/Hsp90 chaperones play an
462 unexpected, inhibitory role in regulating MT stability and neurite growth. In *mec-15(-)* mutants,
463 Hsp70/Hsp90 chaperone and co-chaperones contribute to destabilizing MTs, inhibiting neurite
464 growth, suppressing synaptic development, and disrupting sensory functions. Components of
465 this molecular chaperone machinery include HSP-110/Hsp70, HSP-90/Hsp90, cochaperone
466 STI-1/STI1/Hop (which links Hsp70 and Hsp90), PPH-5/PP5 (which interacts with and
467 activates Hsp90 and other cochaperones through dephosphorylation), DAF-41/p23/ PTGES3
468 (which binds to Hsp90 in its ATP-bound conformation and stabilizes the Hsp90-substrate
469 complexes), and CDC-37/Cdc37 (which interacts with Hsp90 and promote the maturation of
470 kinase substrate) (Figure 6). Removing any of the components in *mec-15(-)* mutants could
471 rescue the TRN developmental defects and restore normal differentiation. The fact that we
472 identified almost every component in a Hsp90 ATPase cycle (or protein folding cycle) suggests
473 that a complete Hsp90 pathway is involved in negatively regulating TRN differentiation.

474 At least part of this negative regulation is mediated by the stabilization of DLK-1,
475 which is a conserved Hsp90 client protein in *C. elegans* (this study), Drosophila, and mice
476 (Karney-Grobe et al., 2018). Because the loss of Hsp90 cochaperones fully rescued all
477 developmental defects in *mec-15(-)* mutants, whereas mutations in *dlk-1* only partially
478 suppressed the neurite growth defects, other client proteins stabilized by Hsp90 chaperones
479 may also participate in the inhibition of TRN differentiation. Future studies will focus on
480 identifying such clients.

481 **Antagonism between UPS and chaperones in neuronal differentiation**

482 Mutations in the chaperones and cochaperones by themselves did not produce any
483 defects in TRN differentiation, suggesting that the inhibitory function of Hsp70/Hsp90
484 chaperones and cochaperones does not seem to affect normal development. This lack of effect
485 may be due to Hsp90 clients, such as DLK-1, being normally maintained at a low level by the
486 UPS involving MEC-15, making the effects of chaperone loss difficult to detect. In *mec-15(-)*
487 mutants, when DLK-1 and likely other Hsp90 client proteins accumulate in the TRNs, they are
488 stabilized by the Hsp70/Hsp90 chaperone machinery and exert their functions. In such
489 scenarios, the activity of chaperones in controlling differentiation became critical. Thus, by
490 targeting the Hsp90 clients for degradation, UPS curbs the activity of the chaperones in
491 inhibiting cellular differentiation.

492 This antagonism between UPS and the chaperones is quite unexpected, since most
493 previous studies indicate that they work synergistically to degrade misfolded proteins. This
494 protein quality control safeguards axon guidance in developing neurons (Wang et al., 2013)
495 and prevents protein aggregation that leads to neurodegeneration (Ciechanover and Kwon,
496 2017). Our studies, however, provide novel insights into the interaction between UPS and
497 chaperones by suggesting that chaperones also promote the expression and stabilization of
498 proteins that are normally degraded by UPS for fast turnover and low background abundance.
499 This tug-of-war keeps the common substrate of UPS and chaperones at the optimal level. This
500 antagonism is crucial for a range of neurodevelopmental processes, including MT formation,
501 neurite growth, synaptic development, and neuronal functions, not only in the TRNs but also
502 in the GABAergic motor neurons. Therefore, we expect that the balance between the UPS and
503 chaperone activities may be important for robust neuronal differentiation in general.

504

505 **Author Contributions**

506 Conceptualization, C.Z. and M.C.; Methodology, C.Z., E.A., K.C.Q.N, D.H.H., and
507 M.C.; Investigation, C.Z., E.A., H.M.T.L, S.L.J.J, and K.C.Q.N; Writing – Original draft and
508 revision, C.Z. and M.C.; Funding acquisition, C.Z., D.H.H., and M.C.; Resource, D.H.H.;
509 Supervision, C.Z. and M.C.

510

Acknowledgements

We thank Natalie Yvonne Sayegh for helping with the *mec-7* suppressor screen and the members of the Chalfie lab for constructive comments on the manuscript. This work is supported by start-up funds from the University of Hong Kong to C.Z. and grants from the Research Grant Council of Hong Kong [ECS27104219 to C.Z.] and the National Institutes of Health of United States [GM30997 and GM122522 to M.C.; OD010943 to D.H.H.]. The electron microscope JEOL 1400Plus TEM used in this study was acquired through a NIH Shared Instrumentation Grant (1S10OD016214-01A1) at Albert Einstein College of Medicine.

Reference

Banz, V.M., Medova, M., Keogh, A., Furer, C., Zimmer, Y., Candinas, D., and Stroka, D. (2009). Hsp90 transcriptionally and post-translationally regulates the expression of NDRG1 and maintains the stability of its modifying kinase GSK3beta. Biochim Biophys Acta *1793*, 1597-1603.

Benitez, M.J., Sanchez-Ponce, D., Garrido, J.J., and Wandosell, F. (2014). Hsp90 activity is necessary to acquire a proper neuronal polarization. Biochim Biophys Acta *1843*, 245-252.

Bounoutas, A., Kratz, J., Emtage, L., Ma, C., Nguyen, K.C., and Chalfie, M. (2011). Microtubule depolymerization in Caenorhabditis elegans touch receptor neurons reduces gene expression through a p38 MAPK pathway. Proc Natl Acad Sci U S A *108*, 3982-3987.

Bounoutas, A., O'Hagan, R., and Chalfie, M. (2009a). The multipurpose 15-protofilament microtubules in C. elegans have specific roles in mechanosensation. Curr Biol *19*, 1362-1367.

Bounoutas, A., Zheng, Q., Nonet, M.L., and Chalfie, M. (2009b). mec-15 encodes an F-box protein required for touch receptor neuron mechanosensation, synapse formation and development. Genetics *183*, 607-617, 601SI-604SI.

Buchberger, A., Bukau, B., and Sommer, T. (2010). Protein quality control in the cytosol and the endoplasmic reticulum: brothers in arms. Mol Cell *40*, 238-252.

Chalfie, M., and Au, M. (1989). Genetic control of differentiation of the Caenorhabditis elegans touch receptor neurons. Science *243*, 1027-1033.

Cheng, P.L., Lu, H., Shelly, M., Gao, H., and Poo, M.M. (2011). Phosphorylation of E3 ligase Smurf1 switches its substrate preference in support of axon development. Neuron *69*, 231-243.

Ciechanover, A., and Kwon, Y.T. (2017). Protein Quality Control by Molecular Chaperones in Neurodegeneration. Front Neurosci *11*, 185.

D'Souza, S.M., and Brown, I.R. (1998). Constitutive expression of heat shock proteins Hsp90, Hsc70, Hsp70 and Hsp60 in neural and non-neural tissues of the rat during postnatal development. Cell Stress Chaperones *3*, 188-199.

Gillan, V., Maitland, K., McCormack, G., Him, N.A., and Devaney, E. (2009). Functional genomics of hsp-90 in parasitic and free-living nematodes. Int J Parasitol *39*, 1071-1081.

Hsu, J.M., Chen, C.H., Chen, Y.C., McDonald, K.L., Gurling, M., Lee, A., Garriga, G., and Pan, C.L. (2014). Genetic analysis of a novel tubulin mutation that redirects synaptic vesicle targeting and causes neurite degeneration in

550 C. elegans. PLoS Genet *10*, e1004715.
551 Ishimoto, T., Kamei, A., Koyanagi, S., Nishide, N., Uyeda, A., Kasai, M., and Taguchi, T. (1998). HSP90 has neurite-
552 promoting activity in vitro for telencephalic and spinal neurons of chick embryos. Biochem Biophys Res Commun
553 *253*, 283-287.
554 Karney-Grobe, S., Russo, A., Frey, E., Milbrandt, J., and DiAntonio, A. (2018). HSP90 is a chaperone for DLK and is
555 required for axon injury signaling. Proc Natl Acad Sci U S A *115*, E9899-E9908.
556 Kim, Y.T., Hur, E.M., Snider, W.D., and Zhou, F.Q. (2011). Role of GSK3 Signaling in Neuronal Morphogenesis. Front
557 Mol Neurosci *4*, 48.
558 Konishi, Y., Stegmuller, J., Matsuda, T., Bonni, S., and Bonni, A. (2004). Cdh1-APC controls axonal growth and
559 patterning in the mammalian brain. Science *303*, 1026-1030.
560 Loones, M.T., Chang, Y., and Morange, M. (2000). The distribution of heat shock proteins in the nervous system
561 of the unstressed mouse embryo suggests a role in neuronal and non-neuronal differentiation. Cell Stress
562 Chaperones *5*, 291-305.
563 Miller, D.J., and Fort, P.E. (2018). Heat Shock Proteins Regulatory Role in Neurodevelopment. Front Neurosci *12*,
564 821.
565 Nakata, K., Abrams, B., Grill, B., Goncharov, A., Huang, X., Chisholm, A.D., and Jin, Y. (2005). Regulation of a DLK-
566 1 and p38 MAP kinase pathway by the ubiquitin ligase RPM-1 is required for presynaptic development. Cell *120*,
567 407-420.
568 Quinta, H.R., and Galigniana, M.D. (2012). The neuroregenerative mechanism mediated by the Hsp90-binding
569 immunophilin FKBP52 resembles the early steps of neuronal differentiation. Br J Pharmacol *166*, 637-649.
570 Richie, C.T., Bembenek, J.N., Chestnut, B., Furuta, T., Schumacher, J.M., Wallenfang, M., and Golden, A. (2011).
571 Protein phosphatase 5 is a negative regulator of separase function during cortical granule exocytosis in C. elegans.
572 J Cell Sci *124*, 2903-2913.
573 Rohl, A., Tippel, F., Bender, E., Schmid, A.B., Richter, K., Madl, T., and Buchner, J. (2015). Hop/Sti1 phosphorylation
574 inhibits its co-chaperone function. EMBO Rep *16*, 240-249.
575 Sato, S., Fujita, N., and Tsuruo, T. (2000). Modulation of Akt kinase activity by binding to Hsp90. Proc Natl Acad
576 Sci U S A *97*, 10832-10837.
577 Schaefer, A.M., Hadwiger, G.D., and Nonet, M.L. (2000). rpm-1, a conserved neuronal gene that regulates
578 targeting and synaptogenesis in C. elegans. Neuron *26*, 345-356.
579 Schmid, A.B., Lagleder, S., Grawert, M.A., Rohl, A., Hagn, F., Wandinger, S.K., Cox, M.B., Demmer, O., Richter, K.,
580 Groll, M.*, et al.* (2012). The architecture of functional modules in the Hsp90 co-chaperone Sti1/Hop. EMBO J *31*,
581 1506-1517.
582 Schwamborn, J.C., Muller, M., Becker, A.H., and Puschel, A.W. (2007). Ubiquitination of the GTPase Rap1B by the
583 ubiquitin ligase Smurf2 is required for the establishment of neuronal polarity. EMBO J *26*, 1410-1422.
584 Singh, V., and Aballay, A. (2006). Heat-shock transcription factor (HSF)-1 pathway required for Caenorhabditis
585 elegans immunity. Proc Natl Acad Sci U S A *103*, 13092-13097.
586 Song, H.O., Lee, W., An, K., Lee, H.S., Cho, J.H., Park, Z.Y., and Ahnn, J. (2009). C. elegans STI-1, the homolog of
587 Sti1/Hop, is involved in aging and stress response. J Mol Biol *390*, 604-617.
588 Sun, Y., Hu, Z., Goeb, Y., and Dreier, L. (2013). The F-box protein MEC-15 (FBXW9) promotes synaptic transmission
589 in GABAergic motor neurons in C. elegans. PLoS One *8*, e59132.
590 Tang, N.H., and Chisholm, A.D. (2016). Regulation of Microtubule Dynamics in Axon Regeneration: Insights from
591 C. elegans. F1000Res *5*.
592 Tedeschi, A., and Bradke, F. (2013). The DLK signalling pathway--a double-edged sword in neural development
593 and regeneration. EMBO Rep *14*, 605-614.

Tuoc, T.C., and Stoykova, A. (2010). Roles of the ubiquitin-proteosome system in neurogenesis. Cell Cycle *9*, 3174-3180.

Uchida, S., Hara, K., Kobayashi, A., Fujimoto, M., Otsuki, K., Yamagata, H., Hobara, T., Abe, N., Higuchi, F., Shibata, T.*, et al.* (2011). Impaired hippocampal spinogenesis and neurogenesis and altered affective behavior in mice lacking heat shock factor 1. Proc Natl Acad Sci U S A *108*, 1681-1686.

Vaughan, C.K., Mollapour, M., Smith, J.R., Truman, A., Hu, B., Good, V.M., Panaretou, B., Neckers, L., Clarke, P.A., Workman, P.*, et al.* (2008). Hsp90-dependent activation of protein kinases is regulated by chaperone-targeted dephosphorylation of Cdc37. Mol Cell *31*, 886-895.

Wandinger, S.K., Suhre, M.H., Wegele, H., and Buchner, J. (2006). The phosphatase Ppt1 is a dedicated regulator of the molecular chaperone Hsp90. EMBO J *25*, 367-376.

Wang, Z., Hou, Y., Guo, X., van der Voet, M., Boxem, M., Dixon, J.E., Chisholm, A.D., and Jin, Y. (2013). The EBAX-type Cullin-RING E3 ligase and Hsp90 guard the protein quality of the SAX-3/Robo receptor in developing neurons. Neuron *79*, 903-916.

Watkins, T.A., Wang, B., Huntwork-Rodriguez, S., Yang, J., Jiang, Z., Eastham-Anderson, J., Modrusan, Z., Kaminker, J.S., Tessier-Lavigne, M., and Lewcock, J.W. (2013). DLK initiates a transcriptional program that couples apoptotic and regenerative responses to axonal injury. Proc Natl Acad Sci U S A *110*, 4039-4044.

Wayne, N., Mishra, P., and Bolon, D.N. (2011). Hsp90 and client protein maturation. Methods Mol Biol *787*, 33-44.

Yamada, T., Yang, Y., and Bonni, A. (2013). Spatial organization of ubiquitin ligase pathways orchestrates neuronal connectivity. Trends Neurosci *36*, 218-226.

Yan, D., and Jin, Y. (2012). Regulation of DLK-1 kinase activity by calcium-mediated dissociation from an inhibitory isoform. Neuron *76*, 534-548.

Yan, D., Wu, Z., Chisholm, A.D., and Jin, Y. (2009). The DLK-1 kinase promotes mRNA stability and local translation in C. elegans synapses and axon regeneration. Cell *138*, 1005-1018.

Zheng, C., Diaz-Cuadros, M., Nguyen, K.C.Q., Hall, D.H., and Chalfie, M. (2017). Distinct effects of tubulin isotype mutations on neurite growth in Caenorhabditis elegans. Mol Biol Cell *28*, 2786-2801.

632

633

634

635 **Figure legends**

636 **Figure 1. F-box protein MEC-15 promotes neurite growth.** (A) The growth of ALM-PN (arrows) in
637 *mec-7(u278 neo)* mutants was suppressed by *mec-15 lf* mutations and was restored in the double mutants
638 by expressing wild-type MEC-15 under a TRN-specific *mec-18* promoter. Arrow head indicates the
639 absence of ALM-PN. (B) Schematic presentation of ALM and PLM morphologies in wild-type and
640 mutant animals with designated neurite names. (C) Protein structures of the wild type MEC-15 with the
641 F-Box and the four WD-40 repeats (WD) labeled in green and blue, respectively. The normalized length
642 (mean ± SD) of ALM-PN in various strains. In all the Figures, error bars represent standard deviation,
643 and asterisks indicate significant difference (* for $p < 0.05$ and ** for $p < 0.01$) in ANOVA and Tukey-
644 Kramer test. (D) TRN morphology in *mec-15(u75 lf)* mutants. (i) low power view (Scale bar = 100 μm).
645 (ii) PLM-AN was shortened and did not extend beyond PVM. (iii) PLM-PN was also significantly
646 shortened. Synaptic branches of (iv) ALM-AN and (v) PLM-AN could not fully extend in *mec-15*
647 mutants. Scale bar = 20 μm in (ii) through (v). (E) The expression of *mec-15::GFP* in (i) anterior and
648 (ii) posterior TRNs, (iii) head neurons, (iv) ventral cord neurons, and (v) the preanal ganglion and the
649 tail.

650 **Figure 2. Loss of Hsp90 chaperones suppress the neurite growth defects in *mec-15 lf* mutants.** (A)
651 ALM-PN is absent in *mec-15; mec-7* mutants (arrow head) and restored in triple mutants *sti-1* and *pph-*
652 *5 lf* mutations (arrow). (B) Schematic presentation of ALM and PLM morphologies in various mutants.
653 *sti-1(-)* is used as an example of *mec-15(-)* suppressors. (C) The length of ALM-PN in various mutants.
654 *hsp-90(ok1333)*, *hsp-1(ok1371)*, and *hsp-110(gk533)* alleles caused larval arrest and were examined at
655 L2/L3 stages. *daf-41(ok3052)*, *sti-1(u1071)*, and *pph-5(u1072)* were examined at both L2/L3 and adult
656 stages; *sti-1(ok3354)* and *pph-5(ok3498)* deletion alleles served as references. *mec-15; mec-7* adult
657 animals carrying transgenes expressing dsRNA against *hsf-1* or *cdc-37* in TRNs were examined; results
658 are labeled as *hsf-1(i)* and *cdc-37(i)*, respectively. (D) Premature termination of ALM-AN and PLM-
659 AN (arrow heads) in *mec-15* single mutants were rescued in *mec-15; sti-1* and *mec-15; pph-5* double
660 mutants. Dashed line indicates the position of the vulva. (E) Shortening of PLM-PN (arrow head) in

661 *mec-15* single mutants were rescued to its normal length (arrows) in the double mutants. (F) Anterior
662 extent of PLM-AN growth in one-day old adults of various mutants grown at 25°C. Distance are given
663 relative to the position of the vulva, so positive values indicate that the PLM-AN grew pass the vulva
664 towards the anterior. (G) PLM-PN length in various mutants. For (F) and (G), *daf-41(ok3052)*, *sti-*
665 *1(u1071)*, *pph-5(u1072)*, *hsp-90(ok1333)*, and *hsp-110(gk533)* were examined. Asterisks indicate
666 statistical significance for the difference between the *mec-7; mec-15* and the triple mutants (C) or
667 between *mec-15* and the double mutants (G) in ANOVA and Tukey-Kramer test.

668 **Figure 3. The loss of MTs and TRN developmental and functional defects in *mec-15* mutants were**
669 **rescued by mutations in Hsp90 cochaperones.** (A) Representative EM micrographs of cross-sections
670 of ALM-AN and PLM-AN in wild-type, *mec-15(u1042)*, *mec-15; pph-5(ok3498)*, and *mec-15; sti-*
671 *1(ok3354)* animals. Scale bar = 100 nm. (B) Average number of MTs in a cross-section of ALM-AN
672 and PLM-AN in various strains. Numbers of sections analyzed for each strain are indicated above the
673 bars. (C) Enlarged EM images of individual MTs with protofilament visualized by tannic acid staining
674 from the cross-sections of PLM-AN of the strains shown in (A). (D) Average diameter of MTs in cross-
675 sections from various strains. Number of MTs measured are indicated above the bars. In (B) and (D),
676 double asterisks indicate statistical significance ($p < 0.01$) for the difference between *mec-15* mutants
677 and the double mutants. (E) Fluorescent intensity of TagRFP in PLM expressed from the *uIs115[mec-*
678 *17p::TagRFP]* transgene in *mec-15(u1042)*, *mec-15; pph-5(ok3498)*, *mec-15; sti-1(ok3354)*, and *mec-*
679 *15; daf-41(ok3052)* mutants. Quantification is in arbitrary units for comparison. (F) Localization of
680 synaptic vesicles labeled by GFP::RAB-3 in TRNs of wild-type, *mec-15*, *mec-15; sti-1*, and *mec-15;*
681 *pph-5* animals. Scale bar = 20 μm. (G) The number of gentle touch responses from five stimuli in the
682 strains indicated. Double asterisks indicate statistical significance ($p < 0.01$) for the difference between
683 *mec-15* mutants and the double mutants.

684 **Figure 4. DLK-1 acts downstream of the chaperones to destabilize MTs and inhibit neurite growth.**
685 (A) Gene structure of the long isoform of *dlk-1* and the position of three *lf* mutations. (B) Normalized
686 neurite length of ALM-PN and PLM-PN in *dlk-1; mec-15; mec-7* triple mutants and the ALM-PN length
687 in the male cross progeny of *mec-15; mec-7* double mutants and *dlk-1(ju476); mec-15; mec-7* triple
688 mutants. Double asterisks indicate significant difference ($p < 0.01$) between the test group and *mec-15;*
689 *mec-7* double mutants. (C) The length of PLM-PN in *dlk-1; mec-15* mutants and wild-type animals

690 expressing *mec-17p::dlk-1a* transgene. (D) The distance between PLM-AN terminal and the vulva in
691 the *dlk-1; mec-15* mutants grown at 25°C. (E) The length of ALM-PN in the indicated mutant animals
692 expressing *mec-17p::dlk-1a* transgene; *dlk-1(ju475)*, *sti-1(ok3354)*, and *pph-5(ok3498)* alleles were
693 used. (F) Yeast two-hybrid assays for the interaction between AD::HSP-90 and BD::DLK-1a. (G)
694 Fluorescent intensity of GFP::DLK-1 expressed from the TRN-specific *mec-17* promoter in wild type,
695 *sti-1(ok3354)*, *pph-5(ok3498)*, and *mec-15(u1042)* mutants and animals carrying *mec-17p::uba-1RNAi*
696 transgenes. Dashed circles enclose PLM cell bodies; scale bar = 20 μm. (H) Fluorescent intensity of
697 TagRFP expressed from *mec-17* promoter in *dlk-1; mec-15* double mutants and in wild type animals
698 expressing *mec-17p::dlk-1a* transgene.

699 **Figure 5. MEC-15 regulates synaptic functions of GABAergic motor neuron by antagonizing the**
700 **activity of Hsp90 chaperones.** (A) Synaptic puncta in the ventral neurite of GABAergic motor neurons
701 labeled by *juIs1[unc-25p::snb-1::GFP]* in the wild-type animal, *mec-15*, *mec-15; sti-1*, and *mec-15;*
702 *pph-5* mutants. (B) Average fluorescent intensity of the SNB-1::GFP puncta in the indicated strains. (C)
703 Average number of SNB-1::GFP puncta in 10 μm of the ventral neurite of GABAergic motor neurons
704 in the indicated strains. (D) Percentage of adult animals paralyzed at the indicated time point after being
705 exposed to 1 mM Aldicarb. Animals were raised from embryos to young adults at either 20°C or 25°C
706 before test. The same *mec-15* data were plotted twice in the two graphs for comparing with the double
707 mutants.

708 **Figure 6. A model for the antagonism between the activities of Hsp70/Hsp90 chaperone machinery**
709 **and MEC-15 in the regulation of TRN differentiation and functions.** HSP-90 receive client protein X
710 from either HSP-110 (a Hsp70 family protein) *via* a STI-1-mediated physical link or CDC-37 via its binding
711 to kinase clients. Both STI-1 and CDC-37 are activated by PPH-5 through dephosphorylation (dashed line).
712 Those Hsp90 client proteins, including DLK-1 and other unidentified proteins (?), are not only stabilized by
713 the chaperones but also subjected to MEC-15-mediated ubiquitination and degradation. Thus, this
714 antagonism between the chaperones and MEC-15 tightly controls the levels of those Hsp90 client proteins,
715 which appear to negatively regulate MT stability, neurite growth, and synaptic development.

716

717

Figure 1

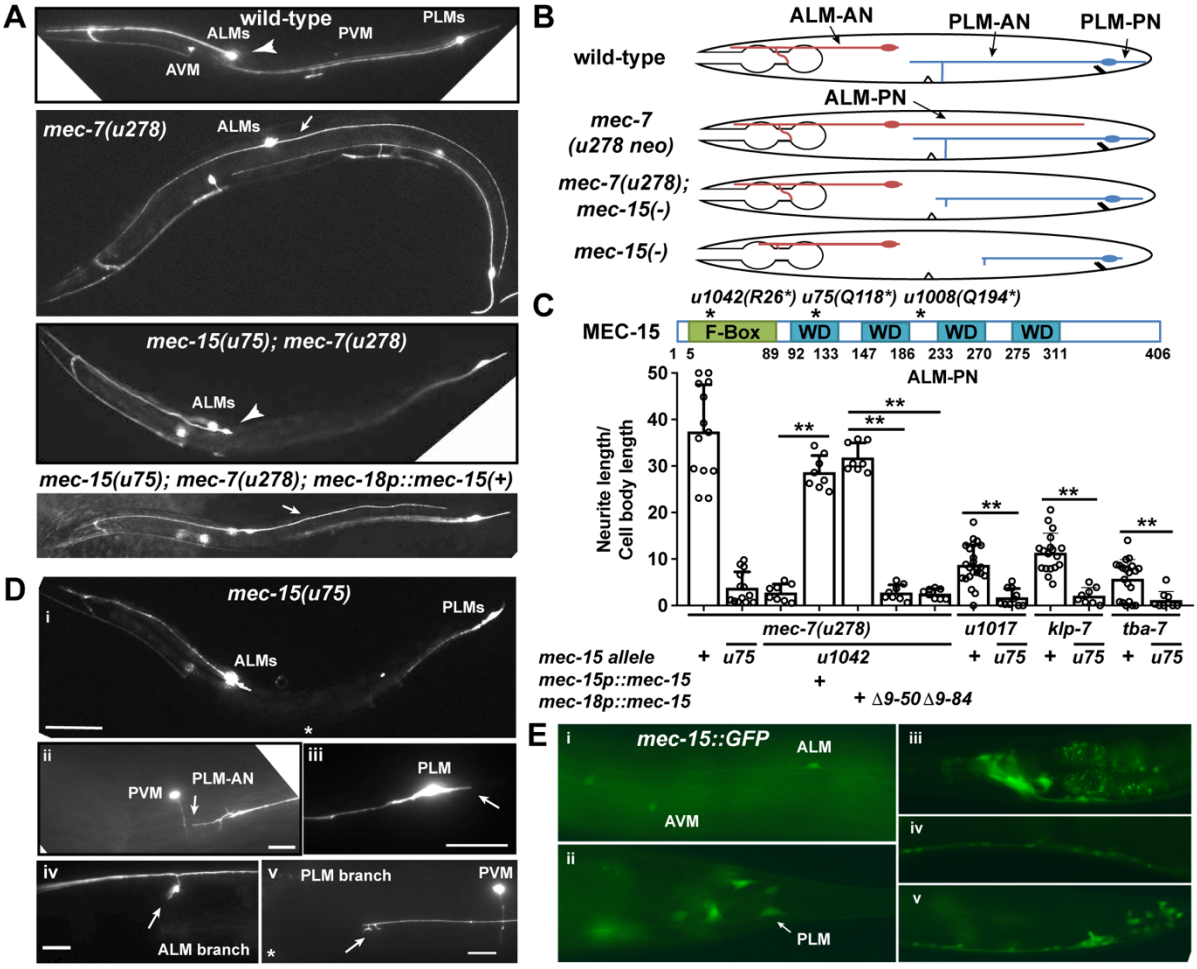
A
wild-type
ALMs
PVM
PLMs
AVM
mec-7(u278)
ALMs
mec-15(u75); mec-7(u278)
ALMs
mec-15(u75); mec-7(u278); mec-18p::mec-15(+)
B
ALM-AN
PLM-AN
PLM-PN
wild-type
ALM-PN
mec-7
(u278 neo)
mec-7(u278);
mec-15(-)
mec-15(-)
C
u1042(R26*) u75(Q118*) u1008(Q194*)
MEC-15
F-Box
WD
WD
WD
WD
1 5 89 92 133 147 186 233 270 275 311 406
ALM-PN
Neurite length/
Cell body length
50
40
30
20
10
0
**
mec-7(u278)
u1017
klp-7
tba-7
mec-15 allele + u75 u1042 + u75 + u75 + u75
mec-15p::mec-15 +
mec-18p::mec-15 + Δ9-50Δ9-84
D
mec-15(u75)
i
ALMs
PLMs
ii
PVM
PLM-AN
iii
PLM
iv
ALM branch
v
PLM branch
PVM
E
i
mec-15::GFP
ALM
AVM
ii
PLM
iii
iv
v

739
740
741 **Figure 2**
742

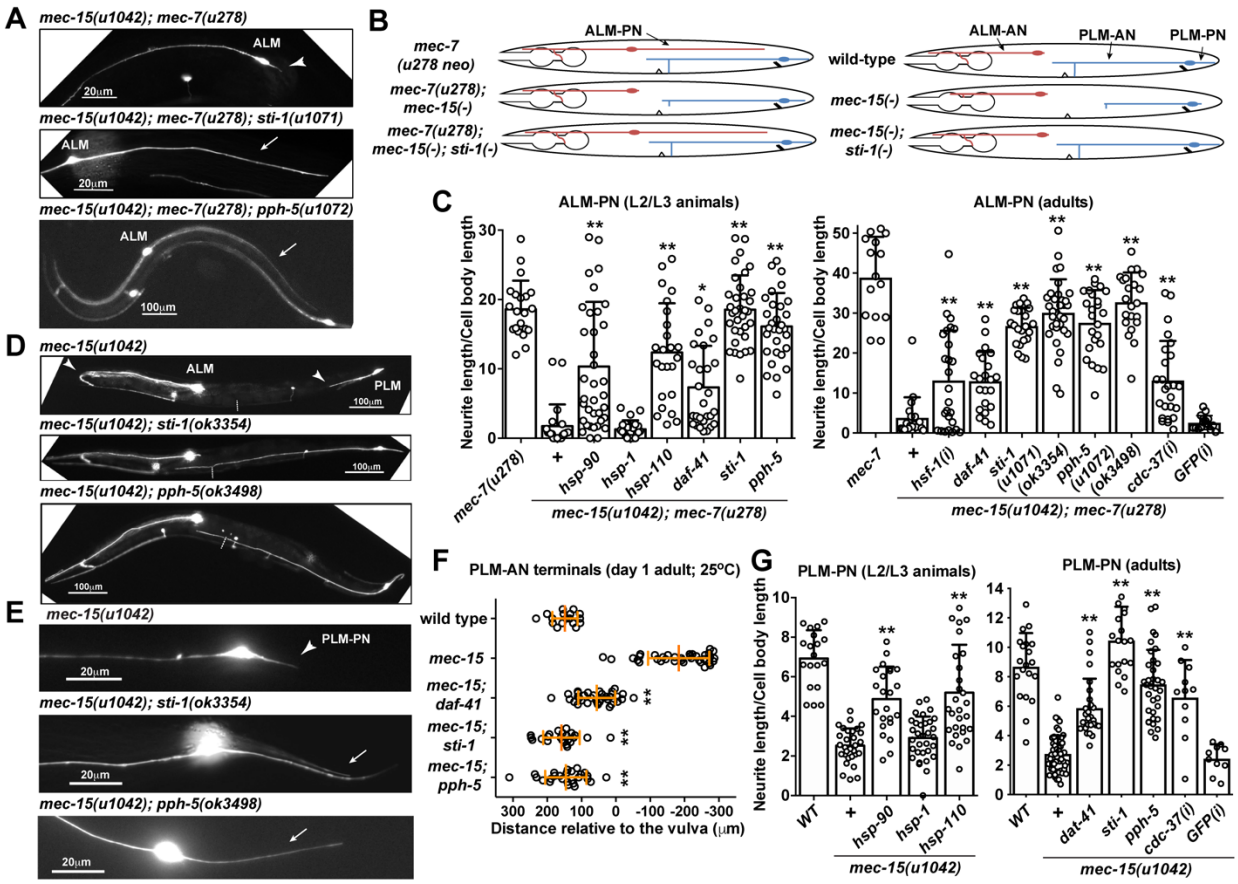

743
744
745
746
747
748
749
750
751
752
753
754
755
756
757
758
759
760
761

762

763 **Figure 3**

764

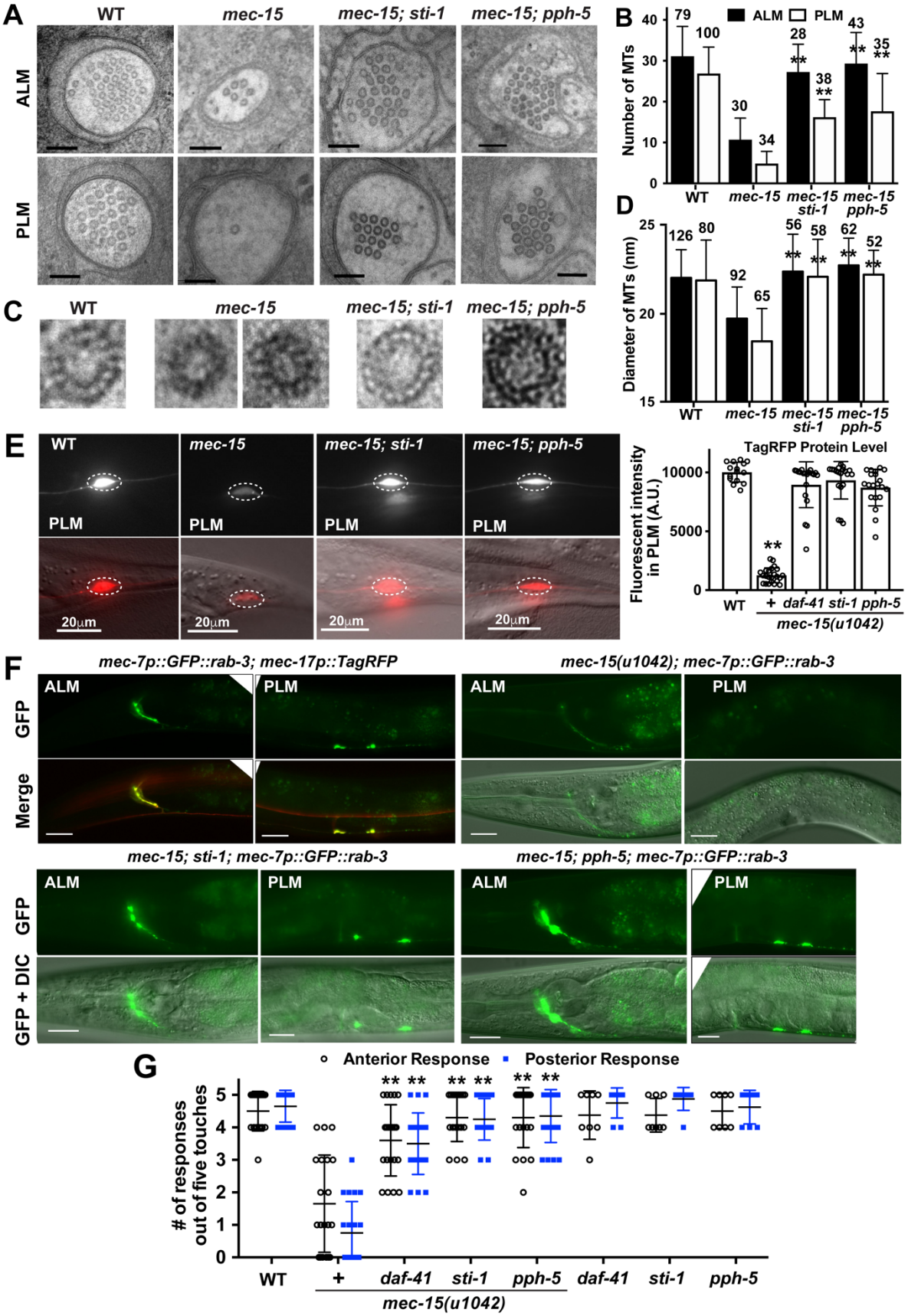

765

Figure 4

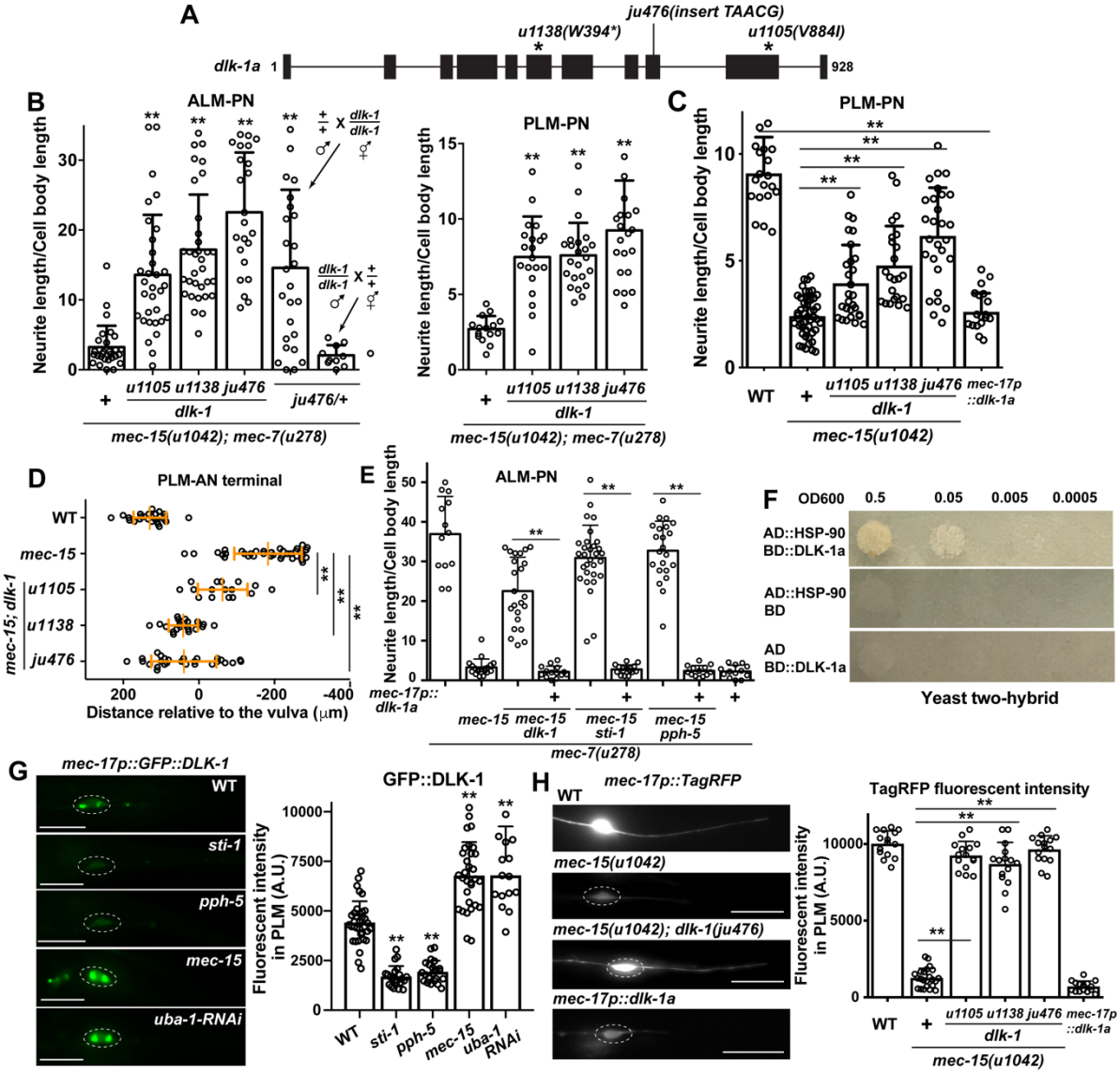
A
ju476(insert TAACG)
u1138(W394*)
u1105(V884I)
dlk-1a
1
928
B
ALM-PN
Neurite length/Cell body length
u1105 u1138 ju476
dlk-1
ju476/+
mec-15(u1042); mec-7(u278)
PLM-PN
C
WT
mec-17p ::dlk-1a
mec-15(u1042)
D
PLM-AN terminal
mec-15; dlk-1
mec-15
u1105
u1138
ju476
Distance relative to the vulva (μm)
E
mec-17p:: dlk-1a
mec-15 mec-15 dlk-1
mec-15 sti-1
mec-15 pph-5
mec-7(u278)
F
OD600
0.5
0.05
0.005
0.0005
AD::HSP-90
BD::DLK-1a
AD::HSP-90
BD
AD
BD::DLK-1a
Yeast two-hybrid
G
mec-17p::GFP::DLK-1
WT
sti-1
pph-5
mec-15
uba-1-RNAi
GFP::DLK-1
Fluorescent intensity in PLM (A.U.)
H
mec-17p::TagRFP
mec-15(u1042)
mec-15(u1042); dlk-1(ju476)
mec-17p::dlk-1a
TagRFP fluorescent intensity

783
784 **Figure 5**
785
786

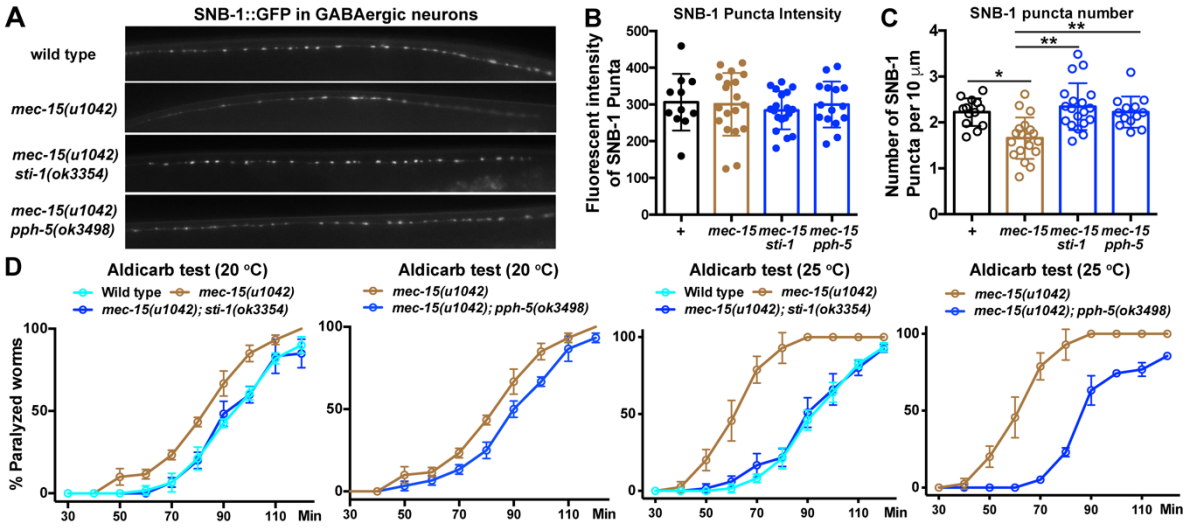

787
788
789
790
791
792
793
794
795
796
797
798
799
800
801
802
803
804
805
806
807
808
809
810
811
812
813
814

Figure 6

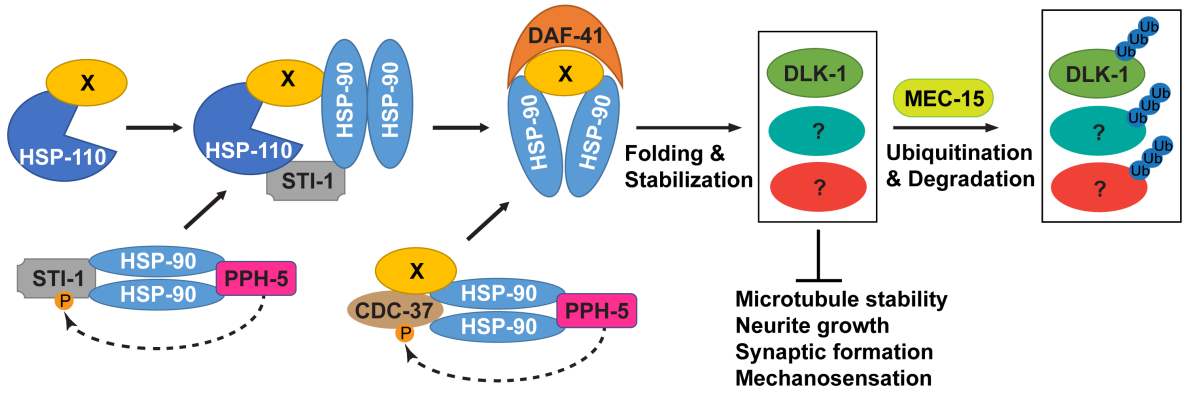
X
HSP-110
X
HSP-110
STI-1
HSP-90
HSP-90
DAF-41
X
HSP-90
HSP-90
Folding &
Stabilization
DLK-1
?
?
MEC-15
Ubiquitination
& Degradation
Ub
DLK-1
?
?
STI-1
P
HSP-90
HSP-90
PPH-5
X
CDC-37
P
HSP-90
HSP-90
PPH-5
Microtubule stability
Neurite growth
Synaptic formation
Mechanosensation